

A tape-reading molecular ratchet

<https://doi.org/10.1038/s41586-022-05305-9>

Yansong Ren¹, Romain Jamagne¹, Daniel J. Tetlow¹ & David A. Leigh^{1,2}✉

Received: 25 May 2022

Accepted: 1 September 2022

Published online: 19 October 2022

 Check for updates

Cells process information in a manner reminiscent of a Turing machine¹, autonomously reading data from molecular tapes and translating it into outputs^{2,3}. Randomly processive macrocyclic catalysts that can derivatise threaded polymers have been described^{4,5}, as have rotaxanes that transfer building blocks in sequence from a molecular strand to a growing oligomer^{6–10}. However, synthetic small-molecule machines that can read and/or write information stored on artificial molecular tapes remain elusive^{11–13}. Here we report on a molecular ratchet in which a crown ether (the ‘reading head’) is pumped from solution onto an encoded molecular strand (the ‘tape’) by a pulse^{14,15} of chemical fuel¹⁶. Further fuel pulses transport the macrocycle through a series of compartments of the tape via an energy ratchet^{14,17–22} mechanism, before releasing it back to bulk off the other end of the strand. During its directional transport, the crown ether changes conformation according to the stereochemistry of binding sites along the way. This allows the sequence of stereochemical information programmed into the tape to be read out as a string of digits in a non-destructive manner through a changing circular dichroism response. The concept is exemplified by the reading of molecular tapes with strings of balanced ternary digits (‘trits’²³), $-1, 0, +1$ and $-1, 0, -1$. The small-molecule ratchet is a finite-state automaton: a special case²⁴ of a Turing machine that moves in one direction through a string-encoded state sequence, giving outputs dependent on the occupied machine state^{25,26}. It opens the way for the reading—and ultimately writing—of information using the powered directional movement of artificial nanomachines along molecular tapes.

The tape-reading molecular ratchet (Fig. 1) consists of a crown ether reading head, **3** (shown in red), that threads through the entry point at the left terminus of a molecular strand (**1** or **2**). This strand contains three compartments separated by acid-labile hydrazone barriers (yellow) to one side and base-labile disulfide barriers (purple) to the other¹⁶. The first and third compartments contain asymmetric *N*-benzyl- α -methylbenzylamine (BMBA; green) groups that are protonated (BMBA-H⁺; blue) in the presence of CCl₃CO₂H or other strong acids such as CF₃CO₂H. The second compartment contains an achiral *N*-methyltriazolium (MT; orange) group²⁷. The relative binding affinities of crown ether **3** are BMBA-H⁺ > MT > BMBA¹⁶. Base catalyses the decomposition of CCl₃CO₂H to CO₂ and CHCl₃ (ref. ²⁸) and so, in the presence of a small amount of triethylamine (Et₃N), a pulse of CCl₃CO₂H changes the pK_a of the environment in which the ratchet operates from basic (Et₃N) to transiently acidic (excess CCl₃CO₂H) and back to basic again (once the CCl₃CO₂H has decomposed). The oscillation in pK_a correlates the opening and shutting of the compartment barriers with a change in the relative affinities of the strand-binding sites for the crown ether, powering an energy ratchet mechanism^{16,22} for directional transport of the crown ether along the molecular strand. The macrocycle exits back into bulk solution from the right terminus of the strand.

When binding to an asymmetric dialkylammonium ion, the 2',2''-quaterphenyl unit of crown ether **3** rotates about the biphenyl bond to adopt the most stable macrocycle conformation for that

particular complex^{29,30}. The resulting spatial arrangement of the axially asymmetric chromophores generates a circular dichroism (CD) response characteristic of the stereochemistry of the bound ammonium group. Binding to an achiral *N*-methyltriazolium group does not induce asymmetry in the macrocycle chromophores. The molecular tape was designed to have minimal absorbance at wavelengths at which the quaterphenyl group absorbs strongly with the stereochemically undefined centres of the disulfide barriers (introduced from racemic building blocks) positioned away from the tape-binding sites. These features help the CD response reflect the effect^{31,32} of binding site stereochemistry on the crown ether, rather than the intrinsic influence of tape stereochemistry on the absorbance of the tape itself. The fuelling synchronizes dynamics so that every macrocycle is at the same tape position simultaneously, resulting in a large and measurable response of the ensemble. Binding to (*R*)- and (*S*)-enantiomers of *N*-benzyl- α -methylbenzylammonium salts yields mirror-image Cotton effects in the absorption region of the quaterphenyl unit^{29,33}. We chose to denote the trits using the balanced ternary system ($-1, +1$ and 0 , rather than $0, 1, 2$ of conventional base 3) so that each digit could be associated with an intuitively suitable chiroptical response of the head²³. The trit encoded by an (*R*)-stereochemistry binding site was chosen to be $+1$ to reflect the sign of the CD spectrum at 280 nm, an (*S*)-stereochemistry binding site -1 and a lack of stereochemistry at binding site 0 . Two pulses of fuel (or two complete acid–base

¹Department of Chemistry, University of Manchester, Manchester, UK. ²School of Chemistry and Molecular Engineering, East China Normal University, Shanghai, China. ✉e-mail: david.leigh@manchester.ac.uk

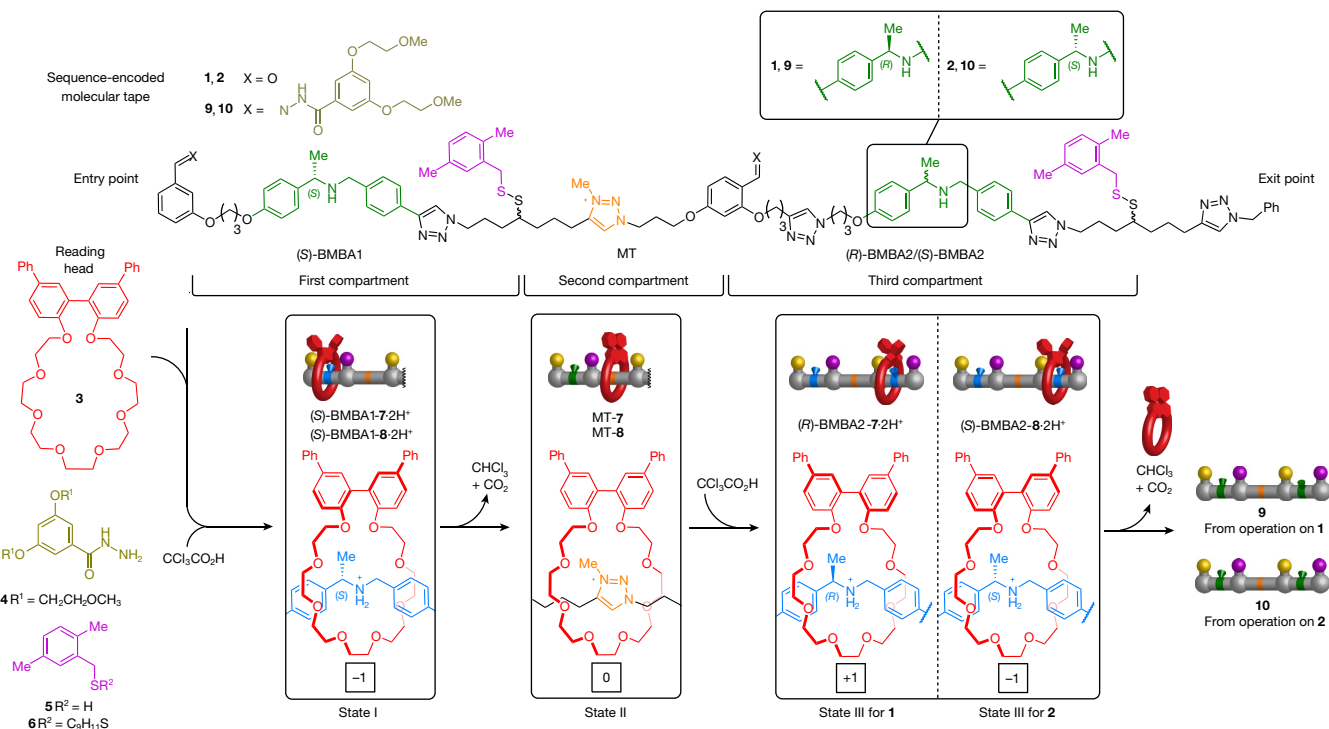


Fig. 1 | Chiroptical readout of the sequence of a stereochemically encoded molecular tape by a chemically fuelled molecular ratchet. Molecular tape **1** features an (*S*)-BMBA- H^+ binding site for crown ether **3** in the first compartment, an MT binding site in the second compartment and an (*R*)-BMBA- H^+ binding site in the third. Tape **2** differs from **1** only in the stereochemistry of the binding site in the third compartment ((*S*)-BMBA- H^+). Prefixes to bold compound numbers indicate the position of the macrocycle on the strand (for example, (*S*)-BMBA1-7 denotes that the crown ether in [2]rotaxane **7** is located in the compartment containing the first BMBA group from the left, and that the BMBA group has (*S*)-stereochemistry). Tape compartments are separated by acid-labile, base-locked hydrazone groups (**4**) on one side and base-labile, acid-locked disulfide groups on the other. Crown ether **3** threads through the entry point at

the left terminus of the tape under acidic conditions (for example, following the addition of $\text{CCl}_3\text{CO}_2\text{H}$) and is transported through the compartments from left to right in response to oscillations in the pK_a of the medium, exiting the tape to the right. As the crown ether passes through the different compartments it changes conformation according to binding site stereochemistry. The different conformations of the crown ether exhibit different CD responses. By monitoring the changing CD spectrum, the sequence of binding site stereochemistries on the tape is read non-destructively by the macrocycle. Tape **1** is encoded $-1, 0, +1$ and tape **2** is encoded $-1, 0, -1$. The molecular ratchet is a finite-state automaton, a machine that runs through a string-encoded state sequence, giving outputs dependent on the occupied state^{24–26}. For an animation of the ratcheting and reading process, see Supplementary Video 1.

oscillations) are required to read a three-trit string of data from **1** or **2** using the molecular ratchet (Fig. 1).

Molecular tapes **1** and **2** and macrocycle **3** were synthesized according to methods described in Supplementary Information (section 3.1). We first operated the machine by the stepwise addition of reagents to allow characterization of each machine state (Extended Data Fig. 1). Trifluoroacetic acid ($\text{CF}_3\text{CO}_2\text{H}$) was added to a solution of tape **1** (80 mM), macrocycle **3** and hydrazide **4** in CH_3CN and stirred for 16 h at room temperature, resulting in the formation of [2]rotaxane (*S*)-BMBA1-7 (the prefix (*S*)-BMBA1 indicates the macrocycle's location on the tape). Treatment with Et_3N kinetically locked the hydrazone groups in place, facilitating the isolation of (*S*)-BMBA1-7 by size-exclusion chromatography. The formation of [2]rotaxane was confirmed by electrospray ionization mass spectrometry (ESI-MS; Extended Data Fig. 1c, top). The location of the macrocycle in the first compartment was confirmed by CD spectroscopy after acidification with $\text{CF}_3\text{CO}_2\text{H}$ (Fig. 2a), which showed a large negative first Cotton effect at λ_{ext} (extremum wavelength) = 282 nm and a second, positive, maximum at $\lambda_{\text{ext}} = 255$ nm, indicative of binding of the crown ether to a BMBA- H^+ site with (*S*)-stereochemistry.

Next, the macrocycle was ratcheted into the middle (*N*-methyltriazolium-containing) compartment. To a solution of (*S*)-BMBA1-7 in CD_3CN were added Et_3N , thiol **5** and disulfide **6**, resulting in the macrocycle passing the labile disulfide barrier (transiently opened by dynamic exchange of the barrier with **5** and **6**) to bind to the MT site (the preferred

accessible binding site, because the BMBA- H^+ groups are deprotonated under basic conditions to BMBA). After 16 h, MT-7 was isolated by size-exclusion chromatography. ESI-MS confirmed the molecule as an isomer of (*S*)-BMBA1-7 (Extended Data Fig. 1c, middle), whereas ^1H NMR spectroscopy indicated that the crown ether was now located in the second compartment (Extended Data Fig. 1b, middle; note the downfield shift of H_b (0.2 ppm) and upfield shifts of H_a (0.2 ppm), H_c (0.5 ppm) and H_d (0.3 ppm)¹⁶.

The addition of $\text{CF}_3\text{CO}_2\text{H}$ and hydrazide **4** to MT-7 in CH_3CN reprotonated the BMBA sites and labilized the hydrazone groups while kinetically locking the disulfide barriers in place. This resulted in the macrocycle being transported into the third compartment to bind to the only accessible dibenzylammonium site, (*R*)-BMBA2- H^+ . [2]Rotaxane isomer (*R*)-BMBA2-7 was isolated after neutralization with Et_3N . The ^1H NMR spectrum of (*R*)-BMBA2-7 (Extended Data Fig. 1b, bottom) is similar to that of (*S*)-BMBA1-7 (Extended Data Fig. 1b, top), but CD spectroscopy confirms that the crown ether in (*R*)-BMBA2-7 is bound to an (*R*)-stereochemistry BMBA- H^+ group and so must be in the third compartment.

The crown ether in (*R*)-BMBA2-7 was released back to bulk off the right exit terminus of the strand by treatment with Et_3N , thiol **5** and disulfide **6** in CD_3CN , affording pristine macrocycle **3** and rereadable tape **1** after one complete operational cycle of the molecular machine (Fig. 1). Molecular tape **2** was operated in a similar stepwise manner to characterize the different machine states (*S*)-BMBA2-8, MT-8 and (*S*)-BMBA2-8.

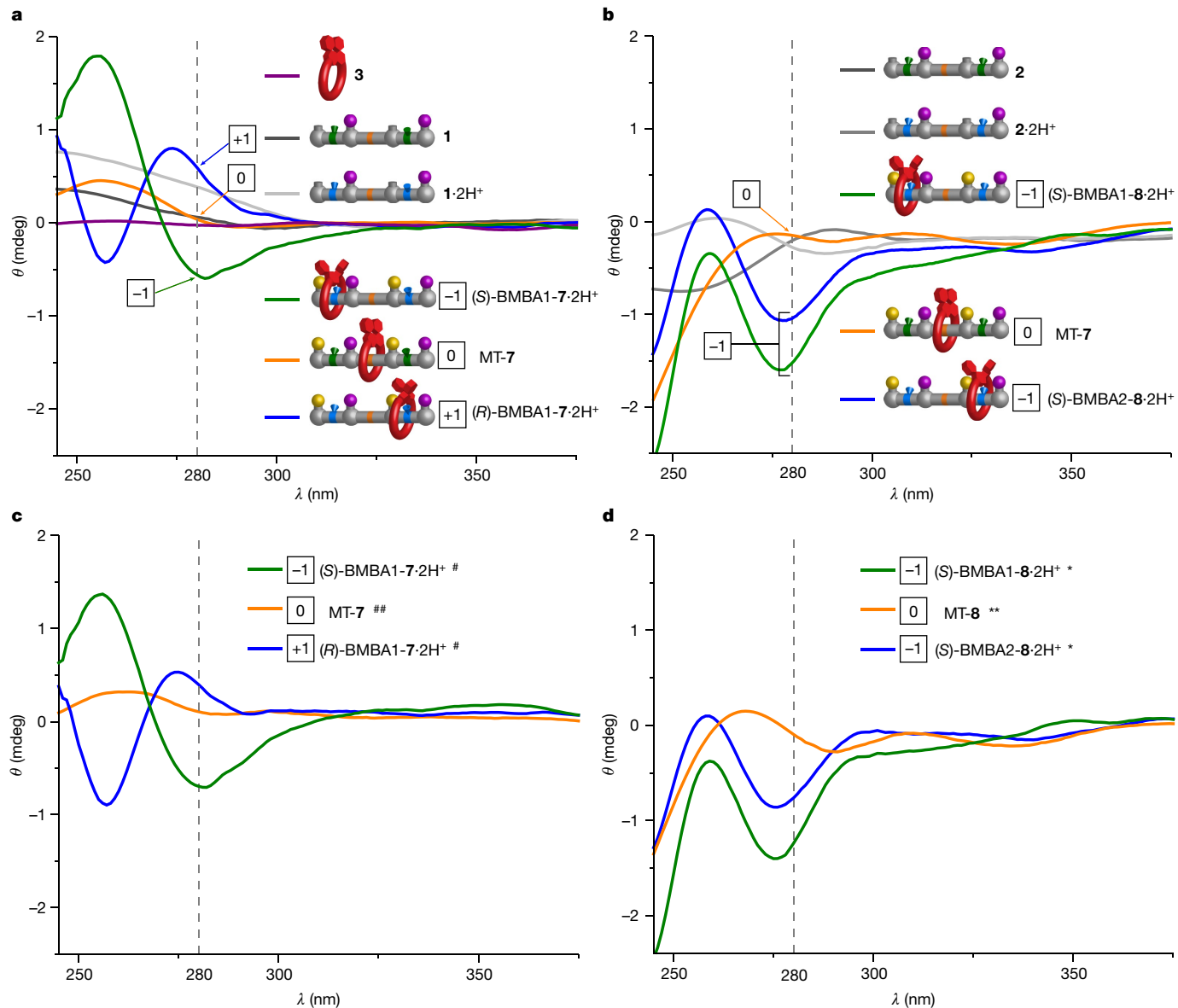


Fig. 2 | CD spectra of the unthreaded components and machine states formed by the stepwise ratcheted operation of **3 along molecular tapes **1** (encoded **-1, 0, +1**) and **2** (encoded **-1, 0, -1**). **a**, CD spectra of components and machine states from the reading of tape **1**. **b**, CD spectra of track and machine states from the reading of tape **2**. **c**, Normalized (# and ##) CD spectra from the**

reading of tape **1**. **d**, Normalized (*) or (**) CD spectra from the reading of tape **2**. θ is the ellipticity in millidegrees (mdeg). # CD spectrum of **1·2H⁺** subtracted; ## CD spectrum of **1** subtracted; * CD spectrum of **2·2H⁺** subtracted; ** CD spectrum of **2** subtracted.

The CD spectra of the different machine states formed during the operations on tapes **1** and **2**, together with those of the unthreaded components, are shown in Fig. 2. Crown ether **3** has $\lambda_{\text{max}} = 256 \text{ nm}$, attributable to quaterphenyl absorption²⁹, but no Cotton effect because the unbound macrocycle is achiral (Fig. 2a, purple line). Tape **1** exhibits a weakly positive Cotton effect at around 250 nm (Fig. 2a, grey line). The threaded structure with the macrocycle in the first compartment of tape **1**, (S)-BMBA1-7·2H⁺, shows a substantially negative Cotton effect at $\lambda_{\text{ext}} = 282 \text{ nm}$ with a second, positive, maximum at $\lambda_{\text{ext}} = 255 \text{ nm}$ (Fig. 2a, green line)^{29,33}. With the macrocycle in the second compartment and binding to the achiral *N*-methyltriazolium group, MT-7, a weakly positive Cotton effect occurs at around 255 nm (Fig. 2a, orange line) similar to that of the unthreaded strand **1** (Fig. 2a, grey line). With the macrocycle in the third compartment, (R)-BMBA2-7·2H⁺, a substantially positive Cotton effect is evident at $\lambda_{\text{ext}} = 274 \text{ nm}$ with a second, negative, band at $\lambda_{\text{ext}} = 257 \text{ nm}$ (Fig. 2a, blue line). The opposite-trending curve profiles

for (S)-BMBA1-7·2H⁺ and (R)-BMBA2-7·2H⁺ confirm that **3** switches conformation to complement the stereochemistry of the binding site. It also shows that the CD signal of [2]rotaxane is substantially amplified compared with that of the unthreaded strand.

Figure 2b shows the CD spectra of the different states that result during the macrocycle's directional transport along tape **2**. Although the machine states with the macrocycle binding to the (S)-*N*-benzyl- α -methylbenzylamine ((S)-BMBA- \cdot H⁺) sites in the first and third compartments ((S)-BMBA1-8·2H⁺ and (S)-BMBA2-8·2H⁺, respectively) have the same shape of CD spectra, the responses are of different intensity, probably a consequence of the flexible strand having different conformations when the macrocycle is located at different regions.

The state of the molecular machine at each position on the tape can be conveniently read out from the CD sign and intensity at 280 nm (vertical dashed line in Fig. 2a,b). In this way, from the order in which the intermediates were formed during the operation of the ratchet, the

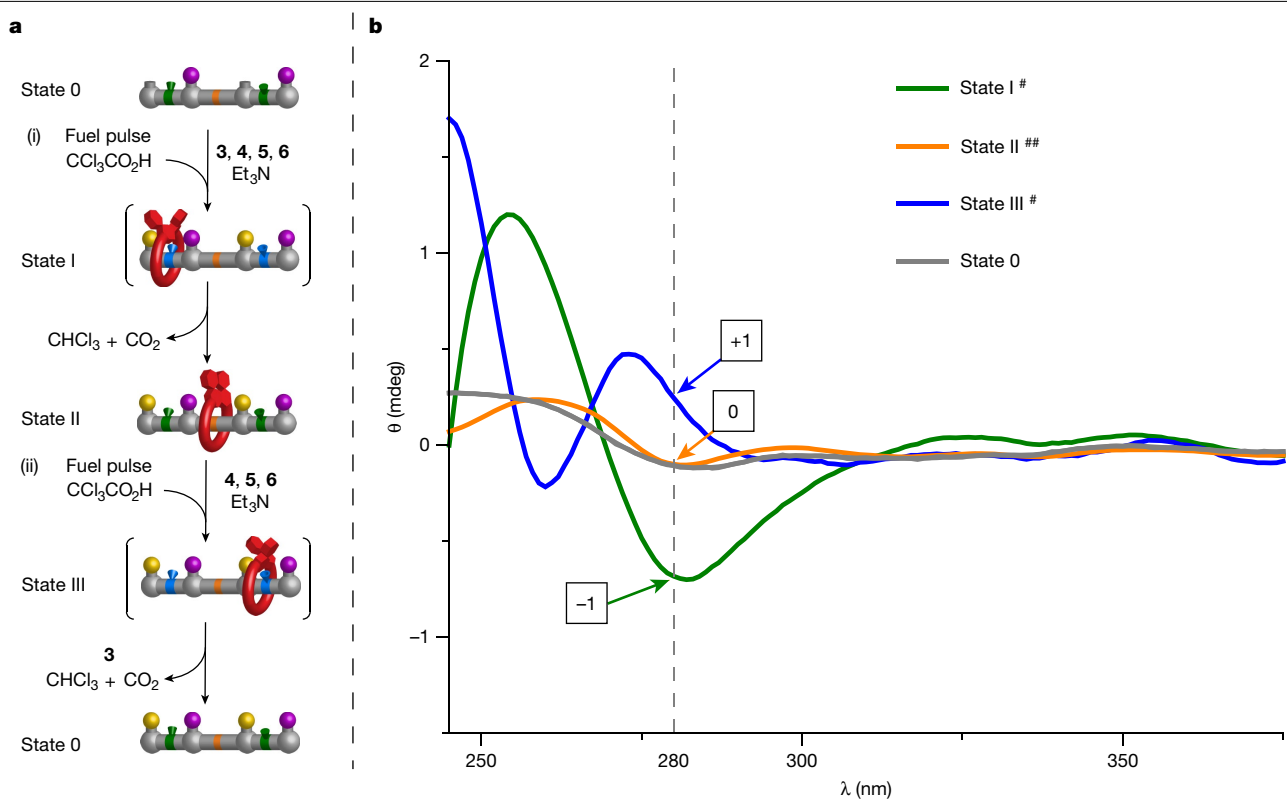


Fig. 3 | Pulse-fuelled reading of molecular tape 1 (encoded $-1, 0, +1$). **a**, Pulse-fuelled transport of macrocycle 3 onto, along and off molecular tape 1: (i) **1** (1.0 equiv.), macrocycle **3** (10.0 equiv.), hydrazone **4** (4.0 equiv.), thiol **5** (1.0 equiv.), disulfide **6** (20.0 equiv.), Et_3N (10.0 equiv.), $\text{CCl}_3\text{CO}_2\text{H}$ (70.0 equiv.) and CH_3CN , rt, 2 d; (ii) $\text{CCl}_3\text{CO}_2\text{H}$ (70.0 equiv.), CH_3CN , rt, 2 d. **b**, Normalized

($\#$ and $##$) CD spectra of samples from state 0 (grey line), state I (green line), state II (orange line) and state III (blue line) during the chemically fuelled operation process. CHCl_3 (**1**/7) = 100 μM . θ is the ellipticity in millidegrees (mdeg). $\#$ CD spectrum of **1** $\cdot 2\text{H}^+$ subtracted; $##$ CD spectrum of **1** subtracted.

string of **1** can be read as $-1, 0, +1$ and that of **2** as $-1, 0, -1$. Alternatively, the CD spectrum of the unthreaded tape can be subtracted from the signal for the ratcheted machine operation to normalize the reading operation, shown for tape **1** in Fig. 2c and for tape **2** in Fig. 2d. Although this does not take into account the differing conformations of the threaded and unthreaded strands, it does compensate to some degree for the local influence of the asymmetric centres on the tape itself. From the shape of the curves and/or the sign and intensity at 280 nm, the strings of **1** and **2** are slightly easier to read (particularly when the crown ether is in the MT compartment) from this normalization of the data (Fig. 2c,d).

With the spectra of the different machine states in hand, we exemplified the use of a pH-switching chemical fuel^{16,17} to power reading through molecular ratcheting by using pulses of $\text{CCl}_3\text{CO}_2\text{H}$ in the sequencing of tape **1** (Fig. 3). The CD spectra of purified samples taken from the reaction 3 h and 2 days after the first fuel pulse, and 3 h and 2 days after the second fuel pulse, are shown in Fig. 3b. The CD spectra were normalized in the same way as seen in Fig. 2c; unsubtracted spectra are provided in Supplementary Information. An excess of $\text{CCl}_3\text{CO}_2\text{H}$ (70 equiv.) was added to a solution of **1** (75 mM), **3**, **4**, **5**, **6** and Et_3N (10 equiv.) in CH_3CN . The fuel protonates the BMBA groups in the tape, allowing the macrocycle to thread and hydrazone barriers to form (Fig. 3a, state I). During this transient acidic period, a sample was taken after 3 h that exhibited a negative first ($\lambda_{\text{ext}} = 282$ nm) and positive second ($\lambda_{\text{ext}} = 256$ nm) Cotton effect (Fig. 3b, green line; similar to the spectrum of (S)-BMBA-7 $\cdot 2\text{H}^+$, Fig. 2c, green line), a reading of ' -1 '. After all of the $\text{CCl}_3\text{CO}_2\text{H}$ had decomposed to CHCl_3 and CO_2 and the reaction mixture had become basic (2 days), a second sample was taken. The CD spectrum of this sample (Fig. 3b, orange line) was similar to that of MT-7 (Fig. 3c), a reading of ' 0 '. A second pulse of fuel was applied to the

material from the first pulse (Fig. 3a, state III). After 3 h an aliquot of the reaction mixture showed a CD response (Fig. 3b, blue line; similar to that of (R)-BMBA-7 $\cdot 2\text{H}^+$; Fig. 2c, blue line), a reading of ' $+1$ '. After a further 2 days the solution had become basic again, and a sample gave a CD spectrum reminiscent of the unthreaded components (state 0; Fig. 3b, grey line), which could then be recovered from the reaction mixture. In the time regime (hours) of fuel decomposition explored here, the rate of macrocycle transport along the tape is determined by the rate of the decomposition of the chemical fuel. If much faster-acting (minutes) pH-switching fuels or conditions are used³⁴, the rate of hydrazone or disulfide barrier exchange could potentially become rate limiting.

In terms of computation theory, the molecular process shown in Fig. 3 corresponds to a finite-state automaton^{24–26}—that is, a machine that runs through a state sequence (here, the sequence of conformational changes of the crown ether) determined by a string of symbols (here, the stereochemistry of the binding sites on the molecular tape). If an absence of stereochemistry is included as a symbol, the string of data in this molecular system can be encoded in trits ($-1, 0, +1$ to reflect the sign of the CD signal at 280 nm, or 0, 1, 2 in conventional base 3 digits). If a lack of CD response is not used as a symbol, the string can be encoded as a binary digit sequence using only BMBA sites.

Tapes **1** and **2** feature trits -1 and $+1$ encoded at BMBA sites and 0 at the MT site. It should be straightforward to encode BMBA-type sites with a zero response (by using an achiral dibenzylammonium group), and we anticipate that -1 and $+1$ may also be encoded at the triazolium site by substitution of the methyl group for chiral alkyl groups. We note the possibility of using differently sized and shaped asymmetric dialkylammonium binding sites (for example, α -isopropylbenzyl-) in addition to BMBA to encode a string with base 5 (or higher-order) digits. The chiral response could be read at multiple wavelengths and,

potentially, with other techniques such as circular polarized luminescence³¹, to maximize sensitivity and discrimination between outputs.

The present ratchet is a finite automaton: a Turing machine that moves in one direction reading information but does not itself automatically record the sequential change in output²⁴. However, switching of the conformation of axially chiral groups has previously been used to change the handedness of products in asymmetric catalysis³⁵. This augurs well for using conformational change in the biaryl unit of the macrocycle to change the stereochemical outcome of a catalysed chemical reaction, so that the molecular ratchet can transcribe information from one form to another as it reads it from a tape. This would be a machine function related to ribosomal transcription in a wholly synthetic molecular system, carried out in a manner reminiscent of Turing's original description¹ of an automatic machine capable of arbitrary computations.

Online content

Any methods, additional references, Nature Research reporting summaries, source data, extended data, supplementary information, acknowledgements, peer review information; details of author contributions and competing interests; and statements of data and code availability are available at <https://doi.org/10.1038/s41586-022-05305-9>.

1. Turing, A. M. On computable numbers, with an application to the Entscheidungsproblem. *Proc. Lond. Math. Soc.* **42**, 230–265 (1936).
2. Bennett, C. H. The thermodynamics of computation—a review. *Int. J. Theor. Phys.* **21**, 905–940 (1982).
3. Adleman, L. M. Molecular computation of solutions to combinatorial problems. *Science* **266**, 1021–1024 (1994).
4. Thordarson, P., Bijsterveld, E. J. A., Rowan, A. E. & Nolte, R. J. M. Epoxidation of polybutadiene by a topologically linked catalyst. *Nature* **424**, 915–918 (2003).
5. van Dongen, S. F. M., Elemans, J. A. A. W., Rowan, A. E. & Nolte, R. J. M. Processive catalysis. *Angew. Chem. Int. Edn Engl.* **53**, 11420–11428 (2014).
6. Lewandowski, B. et al. Sequence-specific peptide synthesis by an artificial small-molecule machine. *Science* **339**, 189–193 (2013).
7. De Bo, G. et al. Sequence-specific β -peptide synthesis by a rotaxane-based molecular machine. *J. Am. Chem. Soc.* **139**, 10875–10879 (2017).
8. De Bo, G. et al. An artificial molecular machine that builds an asymmetric catalyst. *Nat. Nanotechnol.* **13**, 381–385 (2018).
9. McTernan, C. T., De Bo, G. & Leigh, D. A. A track-based molecular synthesizer that builds a single-sequence oligomer through iterative carbon–carbon bond formation. *Chem* **6**, 2964–2973 (2020).
10. Echavarren, J. et al. Sequence-selective decapeptide synthesis by the parallel operation of two artificial molecular machines. *J. Am. Chem. Soc.* **143**, 5158–5165 (2021).
11. Wilson, C. M., Gualandi, A. & Cozzi, P. G. A rotaxane Turing machine for peptides. *ChemBioChem* **14**, 1185–1187 (2013).
12. Varghese, S., Elemans, J. A. A. W., Rowan, A. E. & Nolte, R. J. M. Molecular computing: paths to chemical Turing machines. *Chem. Sci.* **6**, 6050–6058 (2015).
13. Rutten, M. G. T. A., Vaandrager, F. W., Elemans, J. A. A. W. & Nolte, R. J. M. Encoding information into polymers. *Nat. Rev. Chem.* **2**, 365–381 (2018).
14. Erbas-Cakmak, S. et al. Rotary and linear molecular motors driven by pulses of a chemical fuel. *Science* **358**, 340–343 (2017).
15. Biagini, C. & Di Stefano, S. Abiotic chemical fuels for the operation of molecular machines. *Angew. Chem. Int. Edn Engl.* **59**, 8344–8354 (2020).
16. Borsley, S., Leigh, D. A. & Roberts, B. M. W. Chemical fuels for molecular machinery. *Nat. Chem.* **14**, 728–738 (2022).
17. Astumian, R. D. & Derényi, I. Fluctuation driven transport and models of molecular motors and pumps. *Eur. Biophys. J.* **27**, 474–489 (1998).
18. Hernández, J. V., Kay, E. R. & Leigh, D. A. A reversible synthetic rotary molecular motor. *Science* **306**, 1532–1537 (2004).
19. Chatterjee, M. N., Kay, E. R. & Leigh, D. A. Beyond switches: ratcheting a particle energetically uphill with a compartmentalized molecular machine. *J. Am. Chem. Soc.* **128**, 4058–4073 (2006).
20. Cheng, C. et al. An artificial molecular pump. *Nat. Nanotechnol.* **10**, 547–553 (2015).
21. Feng, L. et al. Active mechanisorption driven by pumping cassettes. *Science* **374**, 1215–1221 (2021).
22. Thomas, D. et al. Pumping between phases with a pulsed-fuel molecular ratchet. *Nat. Nanotechnol.* **17**, 701–707 (2022).
23. Davis, M., Sigal, R. & Weyuker, E. J. *Computability, Complexity, and Languages and Logic: Fundamentals of Theoretical Computer Science* 2nd edn (Academic Press, 1994).
24. Hopcroft, J. E., Motwani, R. & Ullman, J. D. *Introduction to Automata Theory, Languages, and Computation* 2nd edn (Addison Wesley, 2001).
25. Benenson, Y., Paz-Elizur, T., Adar, R., Keinan, E. & Shapiro, E. Programmable and autonomous computing machine made of biomolecules. *Nature* **414**, 430–434 (2001).
26. Benenson, Y. Biomolecular computing systems: principles, progress and potential. *Nat. Rev. Genet.* **13**, 455–468 (2012).
27. Coutrot, F. A focus on triazolium as a multipurpose molecular station for pH-sensitive interlocked crown-ether-based molecular machines. *ChemistryOpen* **4**, 556–576 (2015).
28. Abe, Y. et al. Thermoresponsive shuttling of rotaxane containing trichloroacetate ion. *Org. Lett.* **14**, 4122–4125 (2012).
29. Kuwahara, S., Chamura, R., Tsuchiya, S., Ikeda, M. & Habata, Y. Chirality transcription and amplification by [2]pseudorotaxanes. *Chem. Commun.* **49**, 2186–2188 (2013).
30. David, A. H. G., Casares, R., Cervera, J. M., Campaña, A. G. & Blanco, V. A [2]rotaxane-based circularly polarized luminescence switch. *J. Am. Chem. Soc.* **141**, 18064–18074 (2019).
31. Bottari, G., Leigh, D. A. & Pérez, E. M. Chiroptical switching in a bistable molecular shuttle. *J. Am. Chem. Soc.* **125**, 13360–13361 (2003).
32. Jamieson, E. M. G., Modicomb, F. & Goldup, S. M. Chirality in rotaxanes and catenanes. *Chem. Soc. Rev.* **47**, 5266–5311 (2018).
33. Harada, N., Nakanishi, K. & Berova, N. in *Comprehensive Chiroptical Spectroscopy* Vol. 2 (eds Berova, N. et al.) 115–166 (John Wiley & Sons, 2012).
34. Olivieri, E., Gasch, B., Quintard, G., Naubron, J.-V. & Quintard, A. Dissipative acid-fueled reprogrammable supramolecular materials. *ACS Appl. Mater. Interfaces* **14**, 24720–24728 (2022).
35. Wang, J. & Feringa, B. L. Dynamic control of chiral space in a catalytic asymmetric reaction using a molecular motor. *Science* **331**, 1429–1432 (2011).

Publisher's note Springer Nature remains neutral with regard to jurisdictional claims in published maps and institutional affiliations.

Springer Nature or its licensor holds exclusive rights to this article under a publishing agreement with the author(s) or other rightsholder(s); author self-archiving of the accepted manuscript version of this article is solely governed by the terms of such publishing agreement and applicable law.

© The Author(s), under exclusive licence to Springer Nature Limited 2022

Data availability

The data that support the findings of this study are available within the paper and its Supplementary Information, or are available from the Mendeley data repository (<https://data.mendeley.com/>) at <https://doi.org/10.17632/k5m7fv49xv.1>.

Acknowledgements We thank D. Heyes for assistance with CD spectroscopy, the University of Manchester's Department of Chemistry Services for mass spectrometry, the Engineering and Physical Sciences Research Council (EPSRC; grant no. EP/P027067/1) and the European Research Council (Advanced Grant no. 786630) for funding; Marie Skłodowska-Curie Individual Fellowships (no. H2020-MSCA-IF-2020, to Y.R.) and the EPSRC Centre for Doctoral Training in Integrated Catalysis (no. EP/S023755/1, studentship to R.J.); S. D. P. Fielden for

useful discussions; and A. Tanczos (SciComm Studios) for the tape-reading molecular ratchet animation.

Author contributions Y.R., R.J. and D.J.T. planned and carried out the experiments. D.A.L. directed the research. All authors contributed to the analysis of the results and writing of the manuscript.

Competing interests The authors declare no competing interests.

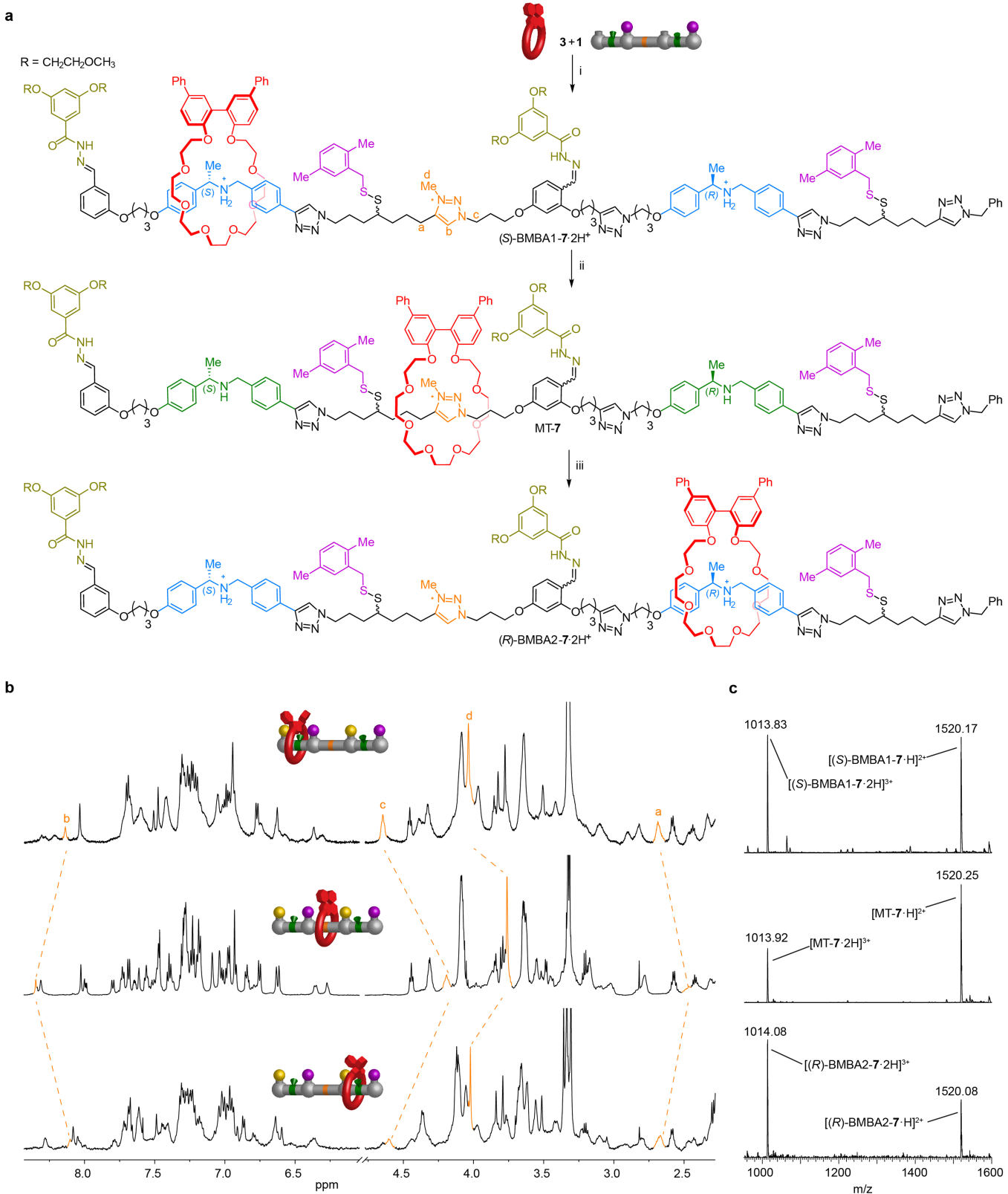
Additional information

Supplementary information The online version contains supplementary material available at <https://doi.org/10.1038/s41586-022-05305-9>.

Correspondence and requests for materials should be addressed to David A. Leigh.

Peer review information *Nature* thanks the anonymous reviewers for their contribution to the peer review of this work.

Reprints and permissions information is available at <http://www.nature.com/reprints>.



Extended Data Fig. 1 | Stepwise ratcheted operation of conformationally flexible crown ether 3 along $-1,0,+1$ stereochemically encoded molecular tape 1. **a**, Reagents and conditions: (i) molecular tape 1 (1.0 equiv.), macrocycle 3 (10.0 equiv.), hydrazide 4 (4.0 equiv.), $\text{CF}_3\text{CO}_2\text{H}$ (6.0 equiv.), CH_3CN , rt, 16 h, then, to allow isolation, Et_3N (50.0 equiv.), 75%. Yields determined after isolation by size-exclusion chromatography. **b**, Partial ^1H NMR (600 MHz, CD_3CN , 298 K) stack plot of [2]rotaxanes (S)-BMBA1-7 (top), MT-7 (middle), (R)-BMBA2-7 (bottom). **c**, Low resolution ESI-MS data for [2]rotaxane (S)-BMBA1-7 (top), MT-7 (middle) and (S)-BMBA2-7 (bottom).

$\text{CF}_3\text{CO}_2\text{H}$ (6.0 equiv.), CH_3CN , rt, 16 h, then, to allow isolation, Et_3N (50.0 equiv.), 75%. Yields determined after isolation by size-exclusion chromatography.

b, Partial ^1H NMR (600 MHz, CD_3CN , 298 K) stack plot of [2]rotaxanes (S)-BMBA1-7 (top), MT-7 (middle), (R)-BMBA2-7 (bottom). **c**, Low resolution ESI-MS data for [2]rotaxane (S)-BMBA1-7 (top), MT-7 (middle) and (S)-BMBA2-7 (bottom).